3D shear wave velocity structure delineation using ambient noise automatic analysis

D. Giannopoulos[1], C. Orfanos[1], K. Leontarakis[1], A. Lois[1] and N. Martakis[1]* show the results of an Ambient Noise Tomography performed in southwest Albania, using long time-series of ambient seismic noise recorded during a Passive Seismic Tomography project, to demonstrate the efficiency and the usefulness of the Passive Seismic Interferometry technique.

Introduction

Passive Seismic Interferometry (PSI) is considered as a revolutionary method characterized by a rapid development especially during the last decade. The method was initially based on the theory that the cross-correlation (CC) of random wave fields of ambient seismic noise recorded on two locations (stations) on the Earth's surface yields an approximation of the Green's function (GF) of the medium between the two locations. The retrieved empirical GF represents an approximation of the seismic response as if one of the two stations was acting as an impulsive source of surface waves (e.g. Claerbout, 1968; Lobkis and Weaver, 2001; Campillo and Paul, 2003; Shapiro and Campillo, 2004; Wapenaar, 2004; Cutris et al., 2006). Since the retrieved GF carries the signature of the velocity structure between the stations, the inter-station travel-times for surface-waves on multiple paths within a seismic network can be used in a tomographic inversion to image the seismic velocity perturbations, by performing the commonly called Ambient Noise Tomography (ANT).

ANT has been widely applied for imaging the velocity structure at continental (e.g. Bensen et al., 2008) and regional scale (e.g. Shapiro et al., 2005) and more recently at local and reservoir scale (e.g. Mordret et al., 2013, 2015). One of the principal advantages of ANT relies on the fact that ambient seismic noise is available almost everywhere on Earth, making ANT totally independent of the spatio-temporal distribution of seismicity. It can provide useful complementary geophysical information for the shallow structures, which sometimes cannot be sufficiently resolved using the classical body-wave tomography, and in some cases, it could be an alternative for exploring seismically quiescent areas. Moreover, ANT is a nondestructive method for seismic imaging, since data are collected without the using active sources, and it is very cost effective.

Aiming to demonstrate the efficiency and the usefulness of PSI technique, an Ambient Noise Tomography was performed in southwest Albania, using long time-series of ambient seismic noise recorded during an already completed Passive Seismic Tomography project (Martakis et al., 2013; Polychronopoulou and Martakis, 2016; Orfanos et al., 2016). More specifically, in the context of this study, an initial estimation of the spatial characteristics of the noise field around the seismic network is provided. Then, the Rayleigh-wave empirical GFs, emerging from CCs of ambient seismic noise between the station pairs, are analysed and the emerging waveforms are used to measure Rayleigh-wave group and phase velocity dispersion curves, in order to obtain 2D group and phase velocity maps at different periods. The group and phase velocity measurements are jointly inverted at various depths, in an attempt to assess the shear-wave velocity distribution of the area of interest. Finally, these results are discussed and evaluated, taking into consideration the outcome of a previously performed Passive Seismic Tomography study in the same area.

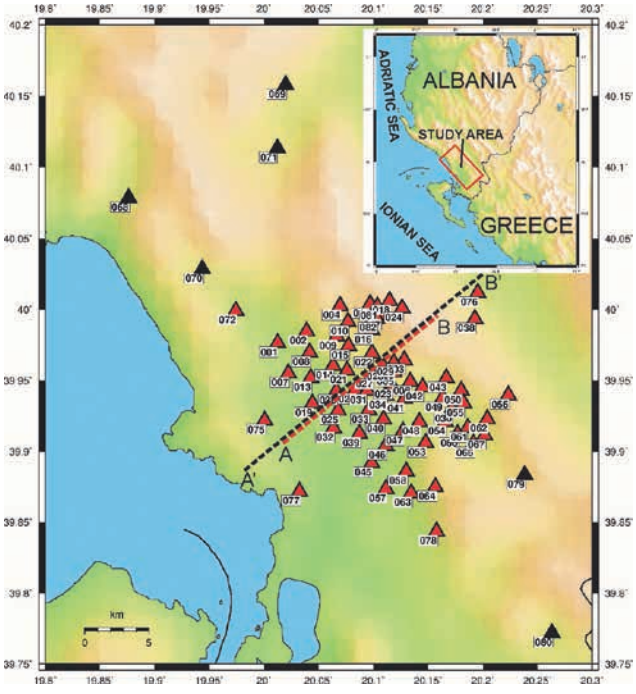

Figure 1 Map of the study area and seismic stations (triangles) deployed during the second phase of a Passive Seismic Tomography survey performed in the area by Seismotech during 2011-2012. The stations used for the present study are displayed with red triangles. The dashed black and red lines denote the location of the geological cross-section and the extracted shear-wave velocity cross-section, respectively, shown in Figure 7.

[1] Seismotech sltd, Athens, Greece
* Corresponding author, E-mail: nmartakis@seismotech.gr

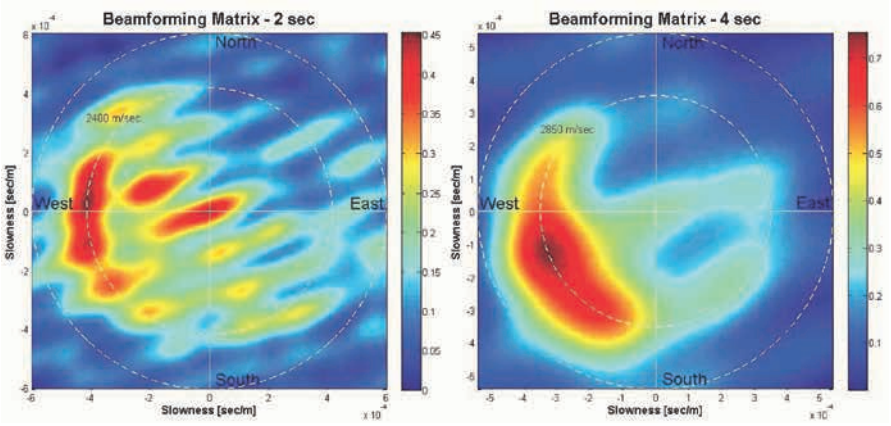

Figure 2 Results of the beamforming analysis for 2 s (a) and 4 s (b) periods. The phase velocities of the maximum amplitude signals are displayed with white dashed circles.

Methodology

Data

In 2011-2012, a Passive Seismic Tomography (PST) project has been carried out by Seismotech. in Delvina area (South Albania). The outcome of this PST project was among others, the construction of detailed 3D P-wave and V_P/V_S models, focusing on both the production and the development area of the Delvina Gas Field. The first phase of the PST project consisted of 50 stations, while the second phase consisted of a significantly denser network of 72 stations covering an area of about 400 km^2 (Figure 1).

From the microseismic network deployed during the second phase of the PST survey, 66 stations (Figure 1) were selected for this study and provided raw data of 60 days continuous recording (11 September to 9 November). The vertical component waveforms were used for the analysis. All seismic stations were equipped with 3-component, 24-bit portable seismic recorders (SR-24) and 3-component shallow borehole seismometers (S-100) with a natural frequency of 4.5 Hz. Recording was continuous with a sampling frequency of 100 Hz.

Distribution of ambient seismic noise sources

Before the necessary processing procedure for the ANT, a beamforming analysis was performed in order to determine, among others, the directionality of the ambient seismic noise sources around Delvina microseismic network. For the beamforming analysis the entire 60-day dataset was used. Initially, the one day-long seismic traces were downsampled to 10 Hz and band-pass filtered between 0.1 and 4 Hz. Downsampling was performed to reduce the data volume and increase the computational speed of the analysis. For each station and for each day, the Fast Fourier Transform (FFT) of the data was calculated. In order to retain only the phase, the signals within each frequency band were normalized by their amplitudes. Plane wave frequency domain beamforming was implemented by following a modified version of the methodology proposed by Brooks et al. (2009). Initially, matrix containing the amplitude normalized short-time Fourier transforms at M=72 stations are constructed and for the i-th day (over N=60 days) is given by $Y_i(t, \omega) = [Y_1(t, \omega), Y_2(t, \omega),.., Y_M((t, \omega)]^T$, $i \in [1, N]$, where t is time, ω is angular frequency and index M refers to the seismic stations. The correlation matrix for the i-th day is estimated according to $C_i = Y_i * Y_i^T$. Thus, for the entire dataset the correlation matrixes C_i are averaged over the N=60 days, $C = \frac{1}{N}\sum_{i=1}^{N} C_i$, concluding to the 'averaged' spatial correlation matrix R which is given by $R = C * C^T$.

Considering with $r_i = (x_i, y_i)$ the coordinates of the sensors as well as with $s(s_x, s_y)$ the slowness vector, a plane wave propagates with, the delay at the i-th station will be $s*r_i$, where r_i is the position relative to the reference station. In the frequency domain, the specific delay is equivalent to a phase shift $\varepsilon = e^{-i\omega(s*r_i)}$. Finally, the output of the beamforming analysis, matrix B, is calculated using the equation $B = \varepsilon^T R \varepsilon$

Figure 2 shows two examples of the beamforming results for the vertical components at 2 s (0.5 Hz) and 4 s (0.25 Hz) periods. Regarding the directions from which Rayleigh-waves of the certain periods arrive at the seismic network, the dominant source regions of the fundamental signals appear to lie between the WNW and WSW of the array. Higher amplitudes are generally observed at a direction ranging between NW and SSW. These source regions are probably related to the water mass of the Adriatic and Ionian Seas and its interaction with the coastlines along the west/southwest of the network.

It is noteworthy to mention that by performing a beamforming analysis, the mean phase velocity dispersion curve of a study area can be efficiently estimated (e.g. Harmon et al., 2008) prior the utilization of the noise correlation functions, providing the possibility to assess an initial 1D shear wave velocity model.

CCs' computation

Before the CCs' computation, a pre-processing procedure was applied station by station on one-day long traces of seismic noise. The pre-processing of our data was performed after adopting a quite standard processing procedure (e.g. Bensen et al., 2007) consisted of the following steps: Removal of the mean and the trend of the signal, decimation of the signal to 5 Hz, band-pass filtering between 0.16-1.2 Hz (0.8-6.25 s), elimination of signal parts with amplitude greater than ten times their standard deviation, spectral whitening, discarding signals with amplitude greater than three times their standard deviation and one-bit normalization.

The daily CCs of the pre-processed noise records between the vertical components of all possible station pairs were calculated and then all daily CCs were stacked over the whole time period, to extract the empirical Rayleigh-wave GFs (reference CCs). Before stacking, daily cross-correlation functions presenting a

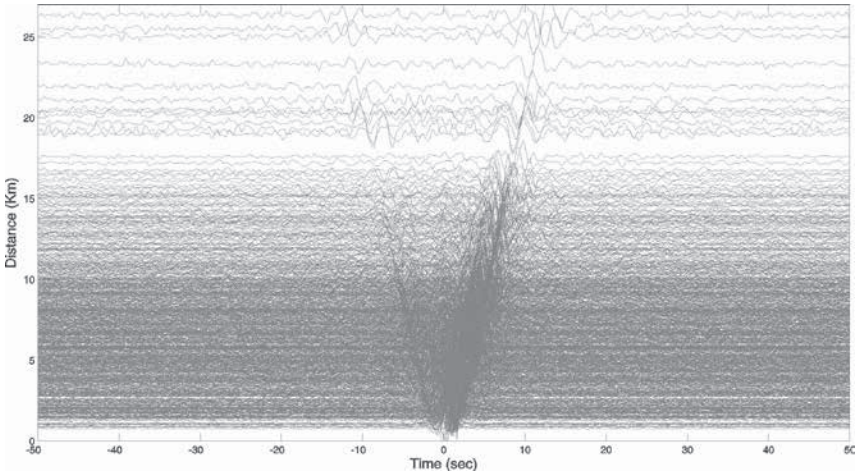

Figure 3 Cross-correlation functions filtered between 0.16 and 1.2 Hz sorted by increasing inter-station distance.

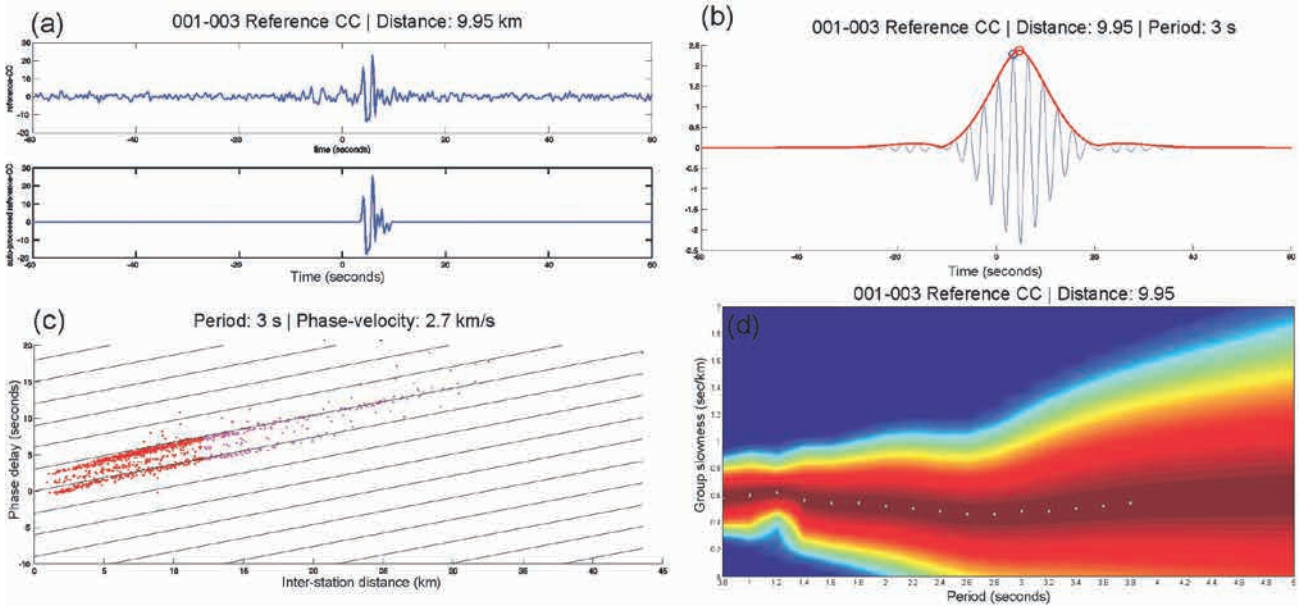

Figure 4 Examples of a) signal's isolation from the reference CC function, b) initial estimation of group and phase delay on a filtered signal at 3 s period, c) diagram of the measured phase delays versus source-receivers inter-station distances (red and magenta dots correspond to inter-station distances less and greater than 1.5 wavelength, respectively) and d) Frequency - Time diagram. White crosses represent the maxima picked by the above mentioned automatic technique.

signal-to-noise ratio (SNR) lower than three were rejected. Finally, for each inter-station CC, the two-sided stacked signals were merged into one-sided by averaging their positive and negative lag times. Figure 3 shows all the computed two-sided cross-correlation functions sorted by increasing inter-station distance. Note the relative asymmetry of the emerged Rayleigh-wave energy between the time lags. An observation which is in agreement with the beamforming outputs indicating possible differences in the distribution of the noise sources radially away from the station-pairs.

Dispersion measurements

Using the reference CCs, the group and phase velocities can be measured as a function of period (frequency) by using the common frequency–time analysis (FTAN) method (Levshin et al., 1989). The automated method adopted in this study, is based on the FTAN method and calculates phase and group velocities on single waveforms without the need of an analyst's interaction. The basic steps of the automated method are analysed in the following paragraphs.

At first stage of the automated analysis, for each reference CC the signal of interest is isolated in the time domain, using an automatically set time window based on inter-station distance and an initial estimate of a minimum and maximum value of group velocities (Figure 4a). An SNR criterion related to the specific time window is applied in order to exclude noisy CCs and unreliable measurements. The next step consists of band-pass filtering of the signals around different frequency bands, and the calculation of the envelope function of each filtered trace.

As a first estimation, the maximum of the envelope of the filtered signal is related to group delay while the maximum of the filtered signal to phase delay (Figure 4b). However, in the case of phase estimation, its use depends on knowledge of the initial source phase and the phase ambiguity term φ_a. For cross-correlations of ambient noise, the source phase is considered to be zero and phase ambiguity term contains a part derived from the 2π ambiguity inherent to any phase spectrum: $\varphi_a = 2\pi N$, where $N = 0, \pm1, \pm2, \ldots$ (Bensen, 2007). Since the above procedure is repeated for all CCs pairs, a diagram of the measured phase delays versus source-receivers inter-station distances is constructed (Figure 4c).

An estimation of a reference phase velocity for each measured period can be derived from the slope of the set of the first order polynomials (starting from the axis origin ±*N* measured periods) that best fits the measured phase delays. Based on the estimated reference phase velocity dispersion curve, a cycle skipping correction is applied at measured phase delays (Jin and Gaherty, 2015).

Moreover, taking also into consideration, the estimated reference phase velocities at each period, an accurate calculation of the wavelengths is carried out, in order to exclude unreliable group delays measurements at frequencies corresponding to inter-station distances larger than 1.5 wavelengths. Averaging the measured group velocities for all reliable inter-station pairs at each frequency, a 'rough' estimation of reference group velocity dispersion curve can be derived. Consequently, without any prior information, it is possible to estimate a reference group and phase velocity dispersion curve of the survey area using only the processed dataset. A comparison of the reference dispersion curves with the beamforming analysis could be an indicator of their reliability. If a priori information exists, such as an 1D shear-wave velocity model of the area, the previous procedure can be skipped and the reference group and phase dispersion curves can be estimated using forward model techniques.

At the final stage, the calculation of group and phase delays is carried out by dynamically setting the parameters of the automated procedure such as the time window for the fundamental energy isolation, the SNR and wavelength versus inter-station distance criterion as well as the rejection of unrealistic phase and group delay measurements. In Figure 4d, an example of the above mentioned automatic technique for the estimation of the group velocity dispersion curve is depicted.

Rayleigh-wave group and phase velocity maps

The tomographic inversions of the group and phase dispersion curves was performed by applying the eikonal equation method (Lin et al., 2009).

For the 2D velocity models (group and phase), a grid with a cell size of $0.01^{o} \times 0.01^{o}$ was used. The Rayleigh-wave group and phase velocities at 22 periods between 0.8 and 5 s (02-1.25 Hz) were used for inversion, with a step of 0.2 s. Following Moschetti et al. (2007), the inversion was performed in a two-step procedure in order to exclude measurement outliers. Measurements having travel-time residuals greater than an upper limit in seconds as well as greater than two times their standard deviation were discarded. For the inversion at each period, the smoothing weight parameters were defined based on SNR. Maps of final 2D Rayleigh-wave group and phase velocity models of the Delvina Gas Field at 2.2 s period are presented in Figure 5.

Depth inversion

The constructed Rayleigh-wave group and phase velocity maps can be considered as a set of local group and phase velocity dispersion curves, respectively. In particular, for each cell of the maps' grid, the group and phase velocity measurements at different frequencies can be gathered, forming with this way local dispersion curves. The joint inversion of a group and a phase local dispersion curve can lead to a local 1D shear-wave velocity model and consequently the combination of all individual 1D models from all grid cells result in the 3D shear-wave velocity structure of the area. 1D profiles as well as 2D vertical and horizontal sections could be extracted from the resulted 3D model, at any desired location or depth, respectively.

For the joint inversion of group and phase velocity dispersion curves a constrained nonlinear least square algorithm has been developed, based on Occam algorithm (Lai, 1998; Constable, 1987). This algorithm solves the nonlinear inverse problem by estimating the shear wave velocity profile given both group and phase velocities dispersion curves (assumed to represent the fundamental mode of propagation) and associated uncertainties. Theoretical dispersion curves of the phase and group velocities as well as the phase velocity partial derivatives with respect to the shear velocity are calculated based on Lai (1998) and Hisada (1994). The partial derivatives of group velocities are computed taking into consideration the phase, group velocities and phase partial derivatives (Rodi et al., 1975). In Figure 6a, the measured phase and group velocity models in comparison to the calculated ones derived by the joint inversion technique are illustrated. Example of jointly inverted local dispersion curves and the corresponding shear wave velocity model, verifying the efficiency of the inversion algorithm, are depicted in Figure 6b, while in Figure 6c the 3D Vs model of the area is presented.

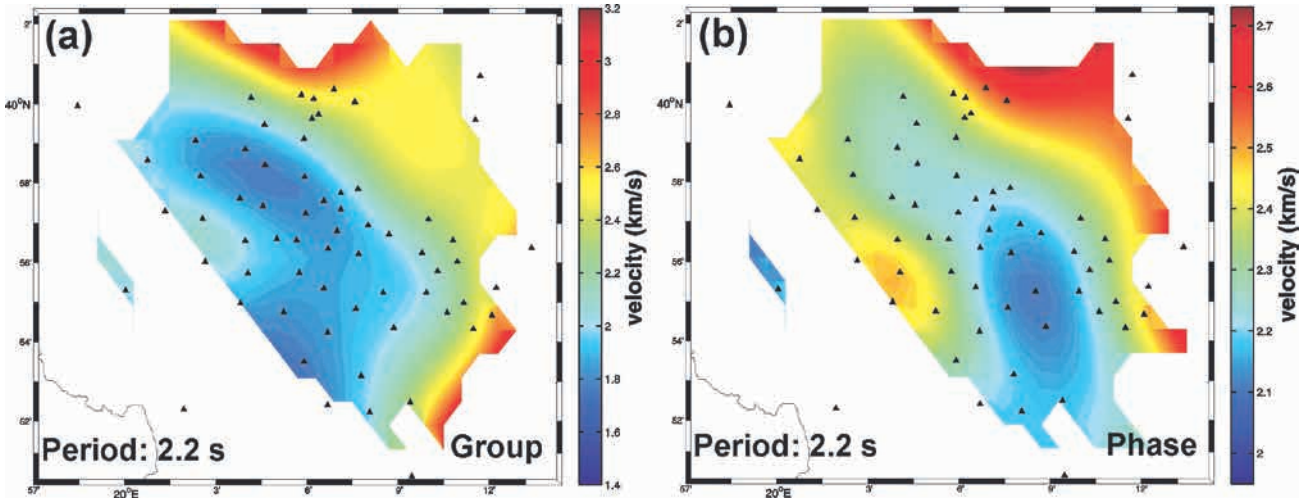

Figure 5 Rayleigh-wave group (a) and phase (b) velocity maps at 2.2 s. Seismic stations are shown as black triangles.

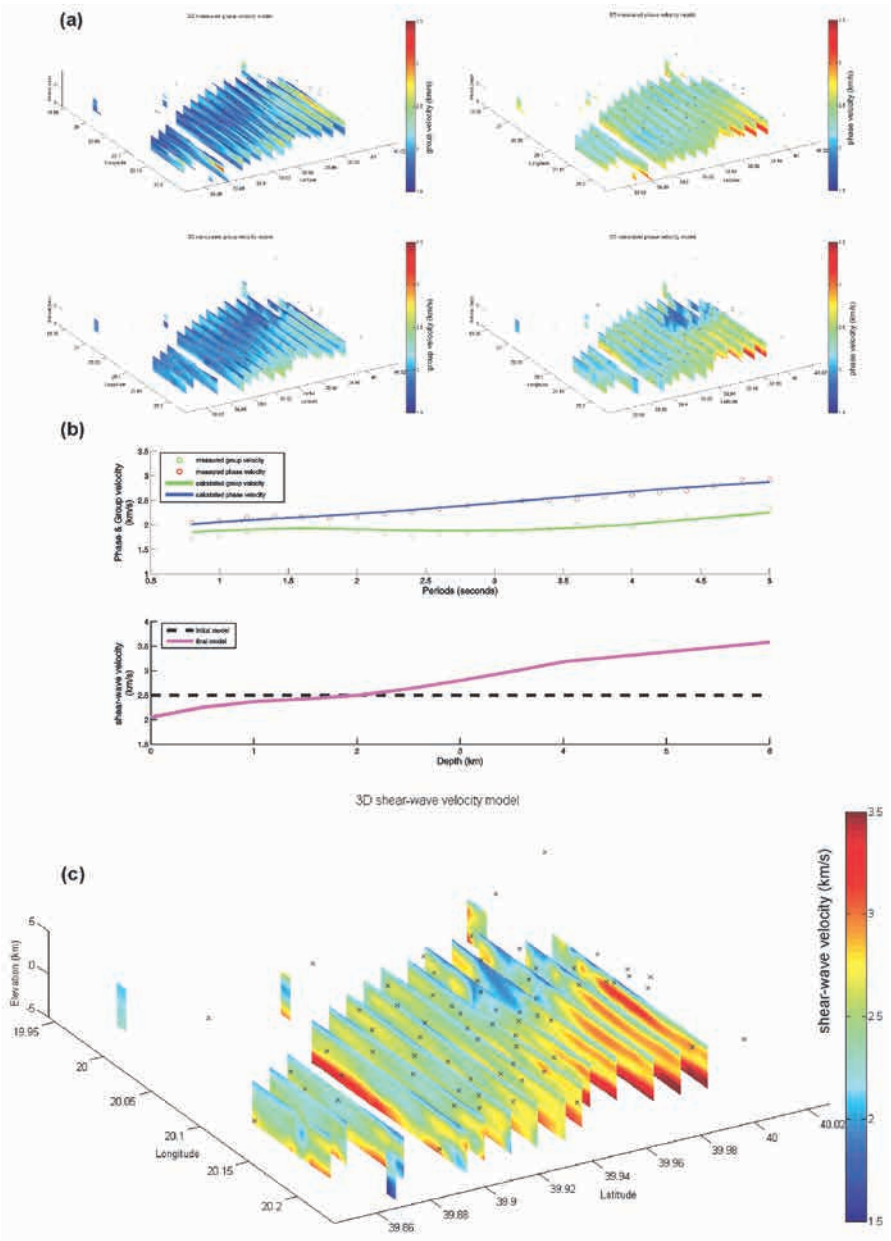

Figure 6 a) 3D measured phase and group velocity models in comparison to the calculated ones, derived by the joint inversion. b) Example of jointly inverted local dispersion curves and the corresponding 1D shear wave velocity model. c) 3D shear wave velocity model of the study area.

Discussion and conclusions

This study emphasizes the usefulness of the seismic interferometry technique as a complementary tool towards the investigation of the velocity structure of the under investigation area in southwest Albania. Sixty days of continuous vertical-component ambient noise data recorded during an already completed Passive Seismic Tomography project in the area were analysed in order to build 2D Rayleigh-wave group and phase velocity maps and asses the 3D shear-wave velocity structure. Since a thorough interpretation of the tomography maps is beyond the scope of this study, the results are briefly discussed in the context of the geotectonic regime of the area, as well as considering the previously performed Passive Seismic Tomography of the study area.

On a broad scale, the results from the Ambient Noise Tomography show a normally expected structure, with the spatial distribution of the higher and lower velocity zones being in a good agreement with the local geotectonic regime. Figure 7 presents a geological cross-section (Velaj, 2015) through the survey area, in which the most prominent tectonic structures are depicted (7a) along with a vertical cross-section extracted from the 3D shear-wave velocity model of our study (7b). The prominent tectonic structures, from west to east, are the Saranda anticline, the Shushica syncline belt, the Ftera-Fitore anticline, the Delvina anticline structure and the Mali Gjere anticline. In general, the observed high velocities are related to the anticline structures which are mostly dominated by carbonates (Velaj, 2015), while lower velocities are associated with the syncline structure of the Shushica syncline belt as well as with the Tertiary (Oligocene flysch and younger Miocene deposits) and Quaternary sediments that overlie these anticline structures (Velaj, 2015). A sufficient spatial correlation is observed between the geotectonic structures and the derived shear-wave velocities from the current study.

The results of the ANT are also evaluated and compared with those obtained by the three-dimensional travel-time tomography study performed during the 2011-2012 PST survey in the

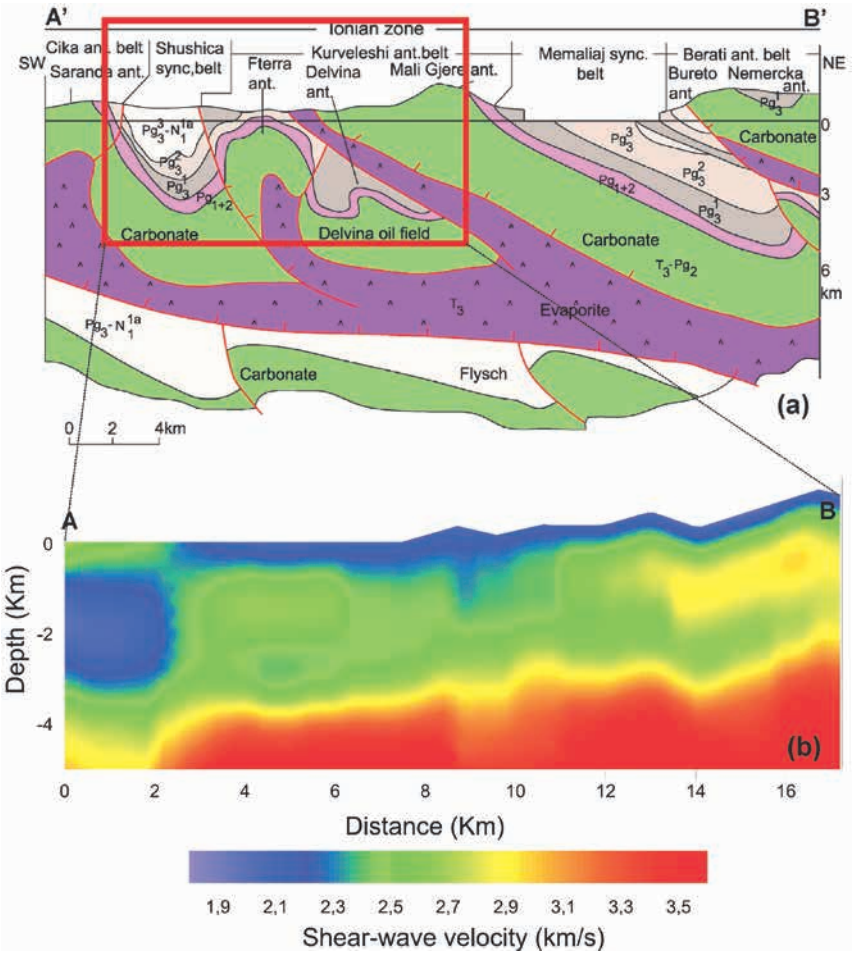

Figure 7 (a) Schematic geological cross-section through the Delvina area (A'B'). (b) Vertical cross-section through the shear-wave velocity model derived from the depth inversion (AB). The spatial correspondence between the shear-wave velocity cross-section and the geological cross-section is depicted by the red rectangle (7a). The geological cross-section is from Velaj (2015). See Figure 1 for the cross-sections' location.

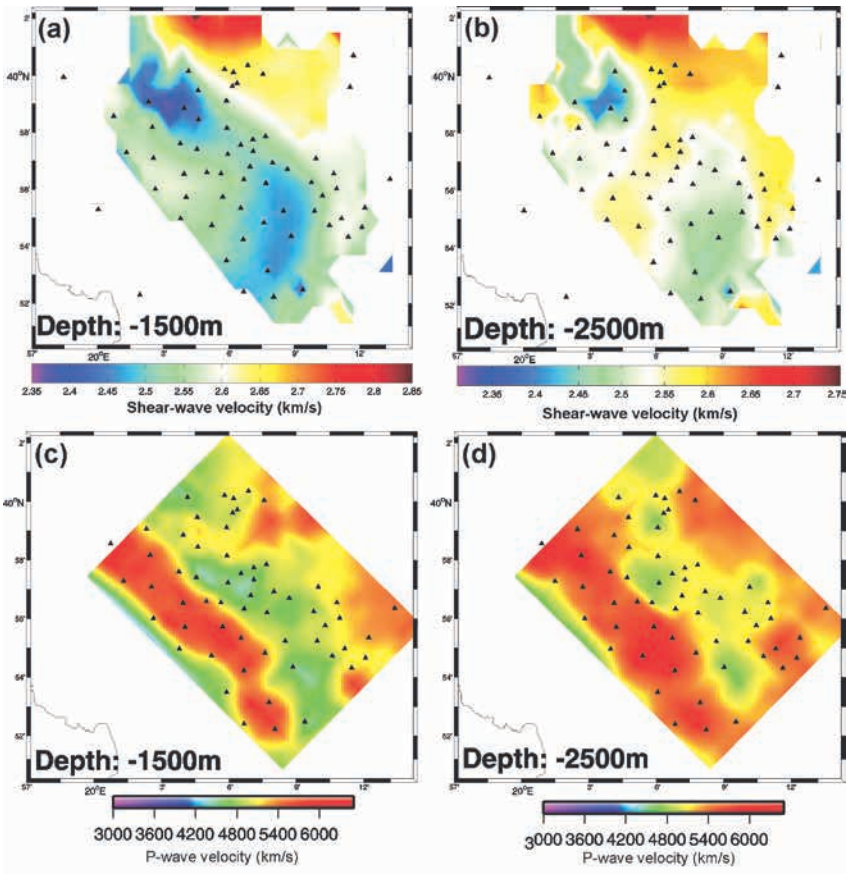

Figure 8 Horizontal cross-sections through the 3D shear-wave velocity model at (a) 1500 m, (b) 2500 m and tomographic models of P-wave velocities around the Delivina area derived by a previous Passive Seismic Tomography survey. P-wave velocity models correspond to the same depths (c) 1500 m and (d) 2500 m.

Delvina Gas Field. As previously mentioned, the outcome of this PST project was the construction of 3D P-wave and V_P/V_S models around the study area. Figure 8 presents two horizontal cross-sections through the 3D shear-wave velocity model at (8a) 1500 m, (8b) 2500 m along with the corresponding horizontal cross-sections through the 3D P-wave velocity model at the same depths (8c and 8d). Making a quite general comparison between the two models, and considering also the different body-wave velocities characteristics (P- and S-wave), large-scale velocity features of our model seem to be similar to those obtained by the travel-time tomography.

Results and conclusions presented in this study can be summarized as follows: (i) a recording time period of two months is sufficiently enough for extracting the necessary information from the ambient seismic noise in order to perform an Ambient Noise Tomography, (ii) it was also demonstrated that despite the fact that the ambient noise sources are not distributed homogeneously around the microseismic network, and consequently despite the asymmetry in the cross-correlation functions, the ambient noise analysis can lead to quite satisfactory results, (iii) in general, Passive Seismic Tomography studies can be significantly improved using information derived from Ambient Noise Tomography, since ANT can provide useful complementary information in addition to P- and S-waves local tomographies in which surface layers are sometimes poorly constrained. It is essential to mention that, the further automation of the above mentioned noise analysis technique, through this study, led among others to the least possible human intervention, increment of the computational speed as well as a more manageable utilization of huge volumes of data.

References

Bensen, G., Ritzwoller, M. and Shapiro, N. [2008]. Broadband ambient noise surface wave tomography across the united states. *Journal of Geophysical Research: Solid Earth*, **113** (B5), 1.

Brooks, L.A., Townend, J., Gerstoft, P., Bannister, S. and Carter, L. [2009]. Fundamental and higher-mode Rayleigh wave characteristics of ambient noise in New Zealand. *Geophysical Research Letters*, **36**, L23303.

Campillo, M. and Paul, A. [2003]. Long-range correlations in the diffuse seismic coda. *Science*, **299**, 547-549.

Claerbout, J.F. [1968]. Synthesis of a layered medium from its acoustic transmission response. *Geophysics*, **33**, 264-269.

Constable, S.C., Parker, R.L. and Constable, G.G. [1987]. Occam's Inversion: A Practical Algorithm for Generating Smooth Models from Electromagnetic Sounding Data. *Geophysics*, **52**, 289-300.

Curtis, A., Gerstoft, P., Sato, H., Snieder, R. and Wapenaar, K. [2006]. Seismic Interferometry – Turning Noise into Signal. *The Leading Edge*, **25** (9), 1082-1092.

Harmon, N., Gerstoft, P., Rychert, C.A., Abers, G.A., Salas de la Cruz, M. and Fischer, K.M. [2008]. Phase velocities from seismic noise using beamforming and cross correlation in Costa Rica and Nicaragua, *Geophysical Research Letters*, **35**, doi:10.1029/2008GL03587.

Hisada, Y. [1994]. An Efficient Method for Computing Green's Functions for a Layered Half-Space with Sources and Receivers at Close Depths. *Bulletin of the Seismological Society of America*, **84** (5), 1456-1472.

Jin, G. and Gaherty, J.B. [2015]. Surface wave phase-velocity tomography based on multichannel cross-correlation. *Geophys. J. Int.,* **201**, 1383-1398, doi:10.1093/gji/ggv079.

Lai, C.G. [1998]. *Simultaneous Inversion of Rayleigh Phase Velocity and Attenuation for Near-Surface Site Characterization.* PhD dissertation, Georgia Institute of Technology.

Lin, F.-C., Ritzwoller, M.H. and Snieder, R. [2009]. Eikonal tomography: surface wave tomography by phase front tracking across a regional broadband seismic array. *Geophys. J. Int.*, **177** (3), 1091–1110.

Lobkis, O.I. and Weaver, R.L. [2001]. On the emergence of the Green's function in the correlations of a diffuse field. *J. Acoust. Soc. Am.*, **110**, 3011-3017.

Martakis, N., Gjoka, M. and Marku, S. [2013]. Passive Seismic Tomography contribution in the delineation of the Delvina Gas Field geological setting. *7th Congress of the Balkan Geophysical Society*, Extended Abstracts.

Mordret, A., Landès, M., Shapiro, N.M., Singh, S., Roux, P. and Barkved, O. [2013]. Near-surface study at the Valhall oil field from ambient noise surface wave tomography. *Geophys. J. Int.,* **193** (3), 1627-1643.

Mordret, A., Rivet, D., Landès, M. and Shapiro, N.M. [2015]. 3D shear-velocity anisotropic model of Piton de la Fournaise volcano (la Réunion island) from ambient seismic noise. *J. Geophys. Res. Solid Earth,* **120** (1), 406-427.

C. Orfanos, Leontarakis, K., Lois, A., Polychronopoulou, K. and Martakis, N. [2016]. Automatic passive seismic data processing with no prior information: the contribution of Surface Wave Tomography. *First Break*, **34** (7), 75-84.

Polychronopoulou, K. and Martakis, N. [2016]. Getting the Most Out of Passive Seismic Tomography: The Case of the Delvina Gas Field Exploration Project. *6th EAGE Workshop on Passive Seismic*, Extended Abstracts.

Ritzwoller, M., Lin, F. and Shen, W. [2011]. Ambient noise tomography with a large seismic array. *Compt. Rendus Geosci.,* **343** (8), 558-570.

Rodi, W.L., Glover, P., Li, T.M.C. and Alexander, S.S. [1975]. A fast, accurate method for computing group-velocity partial derivatives for Rayleigh and Love modes. *Bulletin of the Seismic Society America,* **65**, 1105-1114.

Shapiro, N.M. and Campillo, M. [2004]. Emergence of broadband Rayleigh waves from the correlations of ambient seismic noise. *Geophysical Research Lett*ers, **31** (L07614).

Shapiro, N.M., Campillo, M., Stehly, L. and Ritzwoller, M.H. [2005]. High resolution surface-wave tomography from ambient seismic noise. *Science*, **307**, 1615-1618.

Velaj., T. [2015]. New ideas on the tectonic of the Kurveleshi anticlinal belt in Albania, and the perspective for exploration in its subthrust. *Petroleum*, **1**, 269-288.

Wapenaar, K. [2004]. Retrieving the elastodynamic Green's function of an arbitrary inhomogeneous medium by cross correlation. *Physical Review Letters,* **93** (25), 254-301.